MRS Energy & Sustainability (2023) 10:94–99

doi:10.1557/s43581-022-00055-7

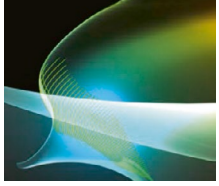

ORIGINAL RESEARCH

SPS sintering and characterization of $Li_7La_3Zr_2O_{12}$ solid electrolytes

Musah Abdulai, Department of Materials Engineering, Sunyani Technical University, Sunyani, Ghana
Kamil Burak Dermenci and **Servet Turan**, Department of Materials Science and Engineering, Eskişehir Technical University, 26555 Eskisehir, Turkey

Address all correspondence to Musah Abdulai at kalamu78@yahoo.com

(Received: 26 July 2022; accepted: 24 October 2022;
published online: 13 December 2022)

ABSTRACT

The key point in this work is the use of spark plasma sintering to reduce the cost of consolidating the powder of lithium lanthanum zirconium oxide solid electrolyte and to study its properties.

In recent years, solid-state electrolyte material such as lithium lanthanum zirconium oxide (LLZO) has become a promising candidate for application in electrical energy storage to replace the liquid electrolyte used in lithium-ion battery technology. Obtaining dense cubic LLZO requires heating of the sample in a furnace at higher temperature for a longer period. This could lead to unwanted evaporation of lithium and excessive cost. Spark plasma sintering (SPS) is used in this study to obtain a dense ceramic cubic LLZO solid electrolyte at temperature as low as 850 °C through solid-state synthesis. This is far lower than the sintering temperature for obtaining cubic LLZO reported in the literature. X-ray diffraction (XRD) patterns exhibit a predominantly cubic phase with minor impurities of pyrochlore and unreacted La_2O_3. The phase composition of the impurities and their effect on ionic conductivity were investigated. The microstructural changes and the density of the pellets obtained were analysed. The trend of the calculated lattice parameter was consistent with the refined lattice parameter. Pellets with relative density as high as 99.9% were produced. The highest ionic conductivity of 4.9×10^{-4} S/cm with activation energy of 0.18 eV was recorded for the sample sintered at 950 °C for 30 min. Compared to the pressureless method of sintering, SPS appears promising for obtaining LLZO cubic phase with higher ionic conductivity at relatively low temperature over a short period.

Keywords ceramic · densification · electrical properties · energy storage · ionic conductor

Discussion

- Lithium-ion batteries have become the preferred choice in many battery technologies. Improving their robustness in terms of energy density and performance is important. This can be done by tackling the chemistry-based issues related to lithium-ion batteries. In fact, among the outstanding features of lithium-ion batteries are their good cycling life and longer life span, which depend on the electrode–electrolyte interface. Safety is another concern when considering practical application, and it lies in the stability of the electrode materials and the internal interfaces. This suggests that the electrolyte is a critical component of a battery system, which limits the application of lithium-ion batteries in most emerging technologies such as electric vehicles.
- Lithium lanthanum zirconate is a solid electrolyte that looks promising compared to liquid-based electrolytes but has challenges such as low ionic conductivity and poor interfacial contact with the electrodes.

Introduction

The recent overwhelming increase in the use of rechargeable lithium-ion batteries for electronic devices such as laptop computers, mobile phones, wearable watches and other miniature electronic devices requires high-safety electrolyte materials with high mobile lithium-ion conductivity. Because of its high lithium-ion conductivity, the liquid organic electrolyte currently used in most lithium-ion batteries poses serious safety challenges including flammability, toxicity and leakage. Solid electrolytes have the potential to resolve these problems, with advantages such as low toxicity, high mechanical performance and safety, as well as design flexibility for batteries. However, the low lithium-ion conductivity and electrochemical stability significantly limit in their application in emerging technologies.[1–5]

Among the Li-ion conducting solid electrolytes reported so far, garnet-structured $Li_7La_3Zr_2O_{12}$ (LLZO) is a promising candidate thanks to its high ionic conductivity at room temperature, good chemical stability with lithium metal and low grain boundary resistance.[6,7] Two types of crystal phases of LLZO have been reported in the literature, cubic and tetragonal.[8–10] The ionic conductivity of the cubic structure is almost three orders of magnitude higher than the tetragonal crystal phase. Over the years, solid-state electrolytes such as LLZO have been sintered through the conventional sintering method. This method is usually time-consuming, as it requires a higher sintering temperature (1200 °C) for a longer period (about 18–36 h)[1,2] and is therefore not cost-effective. During this process, grains become larger, which adversely affects the performance of the LLZO solid-state electrolyte. For this reason, the current study uses spark plasma sintering (SPS) as an alternative sintering technique for LLZO solid electrolyte.

SPS is a fast sintering technique which uses relatively lower temperatures and shorter times to produce a highly dense body.[3,4] The technique has been extensively applied in the successful preparation of dense transparent and structured ceramics, magnetic materials[5,7] and alloys.[7] The advantages of SPS compared to conventional sintering include (a) the use of high heating and cooling rates to reduce the sintering rate and thus conserve energy, (b) ensuring the preparation of high-density ceramic materials with suppressed grain growth at lower temperatures and shorter times, and (c) relatively easy sinterability without the need for sintering aids. During the sintering process, direct current and pressure are simultaneously applied to the graphite die. This produces an increase in the heating process, enabling consolidation of samples within a shorter time at a relatively low temperatures. Mei et al.[11] reported the sintering of $Li_{3x}La_{(2/3-x)}TiO_3$ (LLTO) solid electrolyte with relative density of 98.5% and ionic conductivity of 5.8×10^{-6} S/cm at a sintering temperature of 1050 °C for 3 min. Recently, Zhang et al.[12] reported the sintering of LLZO phase and obtained a cubic phase in a temperature range of 1100–1180 °C over a period of less than 10 min. The study achieved maximum relative density of 99.8% with total ionic conductivity as high as 5.7×10^{-4} S/cm at a sintering temperature of 1150 °C. Similarly, Xue et al.[13] reported total ionic conductivity of 7.6×10^{-6} S/cm when Ta-doped LLZO was sintered by SPS at a fixed temperature of 800 °C, with applied pressure of 40 MPa and holding time of 5 min. In this study, cubic LLZO phase was obtained at a reduced SPS temperature range of 850–1050 °C with comparable total ionic conductivity as high as 4.9×10^{-4} S/cm at 950 °C. The total synthesis time was 90 min, which is comparatively short. This study discusses the microstructure, properties and performance of LLZO sintered by SPS.

Experimental

Synthesis

High-quality Li_2CO_3 powder (99.99%, Merck) was dried at 200 °C for 6 h. Excess of 15% in the form of lithium was added due to the high evaporation of lithium during the heating process. Similarly, La_2O_3 (99.9% Sigma-Aldrich) and ZrO_2 (Inframat, 99.9%) were dried at 900 °C for 6 h to eliminate any hydroxides present. Al_2O_3 was used as an Al source for the stabilization of the cubic phase. A stoichiometric weighed quantity of the starting powders was ground in an agate motor grinder (Retch, RM200) using 2-propanol as grinding medium. The slurry obtained after 90 min of grinding was dried in a rotary evaporator and calcined at 1000 °C for 10 h in an alumina crucible at heating and cooling rates of 3 °C/min and 5 °C/min, respectively. For high homogenization and completeness of reactions, the calcined powder was re-ground for 60 min with the same medium and dried overnight in an oven at 130 °C. For the SPS process, 5 g of the as-prepared powder was filled in the graphite mould with layered carbon paper and placed between two electrodes. The powder was sintered over a temperature range of 750–1050 °C for 30 min with pressure of 13 kN applied. The heating and cooling rates were set to 100 °C/min and 25 °C/min, respectively.

Characterization

The phase identification was carried out with powder X-ray diffraction (XRD; Rigaku MiniFlex 600). Data were acquired at $2\theta = 15°–55°$, a scan rate of 1°/min and a step size of 0.02° with Cu-Kα radiation of λ = 1.5418 Å. A scanning electron microscope (Zeiss Supra 50VP) coupled with an energy-dispersive spectroscopy (EDS) system was used to investigate the morphology of the pellets. The densities of the samples were determined using the Archimedes method in 2-propanol medium. In order to assess electrical properties, a thin film of gold–palladium as Li^+ blocking electrodes was sputtered on the samples for 40 s. Initially, the SPS samples were cut into regular shapes for easy calculation of the area. High-temperature ionic conductivity for the activation energy calculation was determined in a temperature range between 70 and 150 °C. Measurements were taken at temperature intervals of 10 °C and dwell time of 10 min. An alternating-current (AC) impedance method was used in a frequency range from 1 Hz to 1 MHz, with AC perturbation voltage of 30 mV.rms.

Results and discussion

XRD

It can be seen from Fig. 1 that tetragonal phase along with cubic phase were observed for both the calcined powder and the sample sintered at 750 °C, whilst cubic phase was predominantly observed for the sintering temperatures between 850 and 1050 °C, which was lower than pressureless sintering techniques.[1,2] $La_2Zr_2O_7$ (pyrochlore) peaks (in dark grey) and unreacted La_2O_3 peaks (in orange) due to excessive lithium loss were also present and increased with increasing sintering temperature. It can be argued that the excessive evaporation of lithium from the garnet framework during sintering might have led to the formation of pyrochlore, creating more lithium vacancies to allow the incorporation of Al into the garnet framework and stabilizing the cubic phase. However, the lithium vacancy is too high to enable the complete stabilization of the cubic structure.[14,15] It may also be that the time was not sufficient to stabilize the cubic phase, and prolonging the time could lead to lithium loss.

Rietveld refinement analysis was carried out to quantify the phases using GSAS software.[11] Table 1 shows the fraction of phases present according to Rietveld refinement as a function of temperature.

As seen from Table 1, the sample sintered at 750 °C consisted of 41% cubic and 53% tetragonal phases. However, samples sintered at 850, 950 and 1050 °C showed high cubic LLZO phase content, which correlated with the XRD patterns in Fig. 1. The samples sintered at 850 and 950 °C recorded the highest cubic LLZO phase amount, with 84%. However, the amount of cubic LLZO phase was decreased to 78% in the sample sintered at 1050 °C. The continual increase in Li deficit impurity phases such as $La_2Zr_2O_7$, La_2O_3 and $LaAlO_3$ could be attributed to the increased lithium loss with increasing sintering temperature.

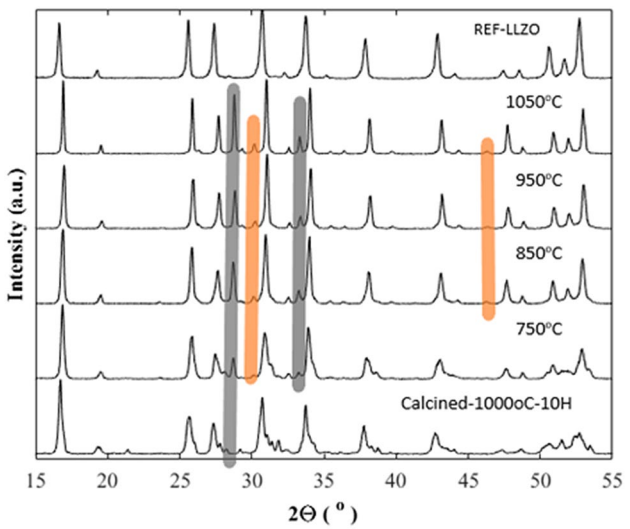

Figure 1. XRD patterns of the calcined powder and SPS samples sintered at 750 °C, 850 °C, 950 °C and 1050 °C for 30 min. Dark grey indicates $La_2Zr_2O_7$ and orange indicates La_2O_3.

Table 1. Phase fraction of the phases present after refinement analysis.

	Phase (%)				
Temp (°C)	cLLZO	tLLZO	$La_2Zr_2O_7$	La_3O_2	$La(AlO)_3$
750	41.0	53.0	7.0	–	–
850	84.0	–	14.0	2.2	0.7
950	84.0	–	13.0	2.6	–
1050	78.0	–	18.4	3.9	–

c = cubic; **t** = tetragonal.

The lattice parameter as obtained from the refinement analysis shows a similar trend (Table 2).

The measured Archimedes density values and lattice parameters are presented in Fig. 2. It is worth noting that data associated with 750 °C is excluded since it contains tetragonal LLZO phase and could be misleading.

The increase in experimental density with increasing sintering temperature was expected during the SPS process, because the occurrence of a high-temperature couple with Joule heating could lead to the intensification of thermal diffusion and migration of the materials along the grains. This results in uniform close contact of the materials and leads to higher densification and sintering. This is also supported by the fractured surface secondary electron images. Although the Archimedes density value may not be the true representation of the actual density due to the closed porosity, visual observations of fractured surface images support the explanation.

The lattice parameter as observed in Fig. 2 decreases as the sintering temperature increases, which confirms the decrease in cell volume recorded after the Rietveld analysis, as seen in Table 2.

This could mean that the phase transformation from tetragonal to cubic is accompanied by decrease in expansion of the structure as seen in the values of cell volume and the higher magnitude of the lattice parameter, which is consistent with the literature (Fig. 3).[13,16]

The fractured surface secondary electron image of the sample sintered at 950 °C appeared to show uniform grains with compact distribution among the particles, whilst the sample sintered at 1050 °C exhibits larger grains with few smaller grains. Except for the sample sintered at 950 °C, all the samples showed inner voids, which reflects the ionic conductivity recorded.

Electrical properties

The electrochemical impedance spectroscopy (EIS) response obtained from the sample which showed a cubic phase is presented in Fig. 4.

Table 2. Rietveld refinement values of lattice constant, volumes, R_{wp} values, goodness of fit (GOF) and the estimated standard deviation (esd) for the samples sintered at 750, 850, 950 and 1050 °C for 30 min at pressure of 13 kN.

Temp (°C)	Lattice constant (Å)	Volume (Å^3)	*R* value (R_{wp}) (%)	GOF
750 *esd*	a = 13.061314 c = 12.755349 *a = 0.003100* *c = 0.002580*	2176 *1.370*	17.36	2.06
850 *esd*	12.969642 *0.001838*	2182 *0.928*	16.68	1.90
950 esd	12.965122 *0.001435*	2179 *0.723*	15.19	1.64
1050 *esd*	12.961090 *0.000793*	2175 *0.399*	15.83	1.76

The italics is just to differentiate the esd from the actual values.The R values and the GoF values are to indicate how the observed data align with the expected values after the rietveld refinement. The esd is the error margin or the deviation from the expected values that is the lattice constant and volume

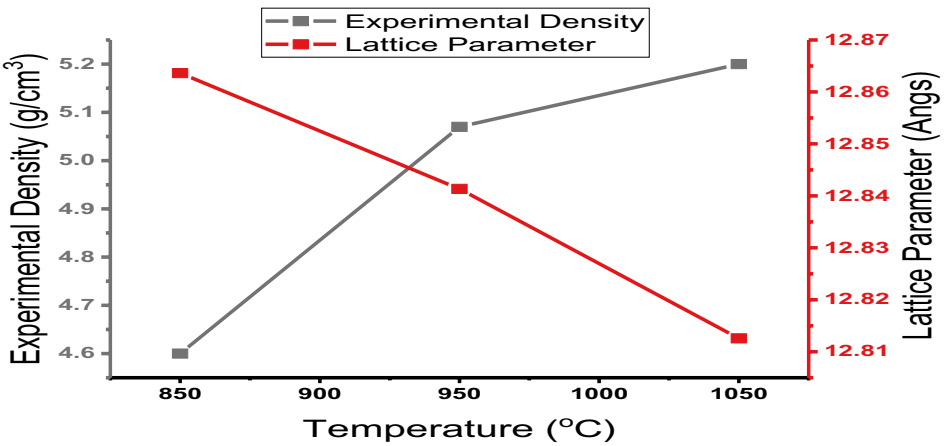

Figure 2. Experimental densities and lattice parameters as a function of sintering temperature for LLZO sintered by SPS.

The fitting of the curves was carried out by the ZView program with the equivalent circuit model consisting of three constant phase elements (CPE) each in parallel connection with a resistor, as shown in the inset of Fig. 4. As seen in Fig. 4, the Nyquist plots showed two semicircles at high frequency for the sample sintered at 850 °C, indicating the contribution of both the bulk and grain boundary to the total ionic conductivity of the samples. The 950 °C and 1050 °C samples exhibited a single semicircle. The appearance of the tail in the low-frequency region of the response was due to the sputter coating of Au–Pd Li-ion blocking electrodes. According to the fitted data obtained from Nyquist curves, the total ionic conductivity values measured at room temperature for the samples sintered at 850 °C, 950 °C and 1050 °C are 2.5×10^{-5} S/cm, 4.9×10^{-4} S/cm and 5.5×10^{-5} S/cm, respectively. The appearance of non-conductive impurities such as $La_2Zr_2O_7$, La_2O_3 and the less conductive $LaAlO_3$ could have dramatically decreased the electrolyte ion conductivity. According to a similar study by Xue et al.,[13] the decrease in ionic conductivity is primarily due to the formation of non-conductive $La_2Zr_2O_7$ impurity. In their article, Joong et al.[17] also asserted that the formation of $La_2Zr_2O_7$ led to a higher activation energy of 0.67 eV and a two- to three-order reduction in conductivity.[18] From the results of first-principles calculations, the $La_2Zr_2O_7$ pyrochlore materials have very stable electronic properties with a wide band gap, making them insulative.[19] Castillo et al.[16] also obtained high activation energy values, resulting from the contribution of the less conductive $LaAlO_3$ impurity. From Table 1, the sample with the higher impurity values has the lowest ionic conductivity value, which is in accord with results reported in the literature.

The grain boundary conductivity is lower than bulk conductivity for the sample sintered at 850 °C. However, with increasing temperature, the gap between bulk and grain boundary conductivity increased. Such behaviour could be attributed to the enhanced densification and relatively low contribution of grain

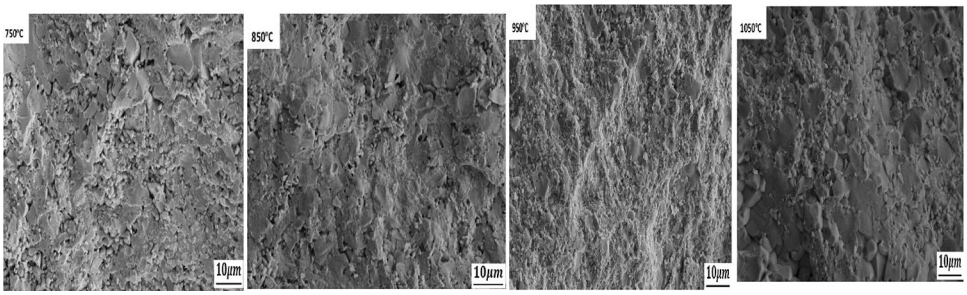

Figure 3. Scanning electron microscopy (SEM) images of fractured surfaces of SPS samples sintered at 750 °C, 850 °C, 950 °C and 1050 °C for 30 min.

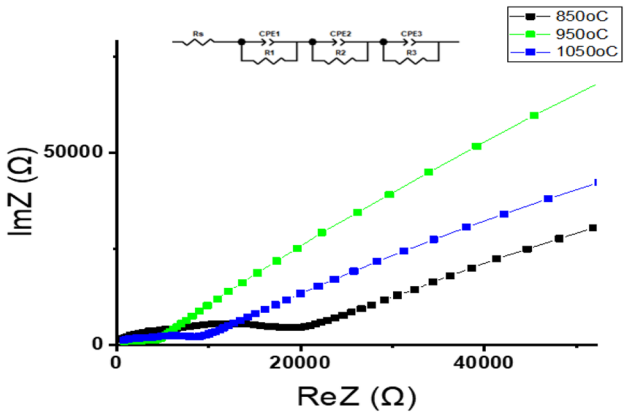

Figure 4. Typical Nyquist plot for the sample sintered by SPS.

boundary conductivity to total conductivity. Figure 5b shows the activation energy and total conductivity values as a function of temperature.

The activation energy indicates the ease of Li transport in solid electrolytes. Therefore, evaluation of activation energy is important for complete evaluation of solid electrolyte performance. The graphical representation of high-temperature ionic conductivity, as illustrated in Fig. 5a, indicates that all three samples share common problems of low ionic conductivity caused by impurities. Also, it confirms the assertion that conductivity is thermally controlled at high temperature, which may lead to a different degree of interaction between defect pairs and differences in vacancy concentrations. The Arrhenius curves as observed in Fig. 5a display a decrease in electrolyte ionic conductivity as temperature increases, which suggests that the temperature increase energized the conductible lithium ion, enabling it to break through the migration barrier. At higher temperature, the conductivity observed decreases slightly, which indicates that at higher temperature, the effect of temperature on ionic transport is non-significant. At these temperatures, lithium has enough energy to migrate. The calculated activation energy values are 0.94 eV (850 °C), 0.18 eV (950 °C) and 0.46 eV (1050 °C), which are similar to those reported previously.[12,16,20,21] The small activation energy value recorded for the sample sintered at 950 °C indicates that the energy needed for lithium ion migration decreases, thus increasing the ionic conductivity. The high value of impurities recorded for the rest might have contributed to the increase in the activation energies, which decreased the ionic conductivity.

Despite the presence of the Li-deficit phases in the Al-stabilized LLZO sintered by SPS, the present study reported total ionic conductivity of 4.9×10^{-4} S/cm for the sample sintered at 950 °C, which is one of the highest conductivity values reported in the literature at temperatures higher than the 950 °C used in this study.[11,13,15]

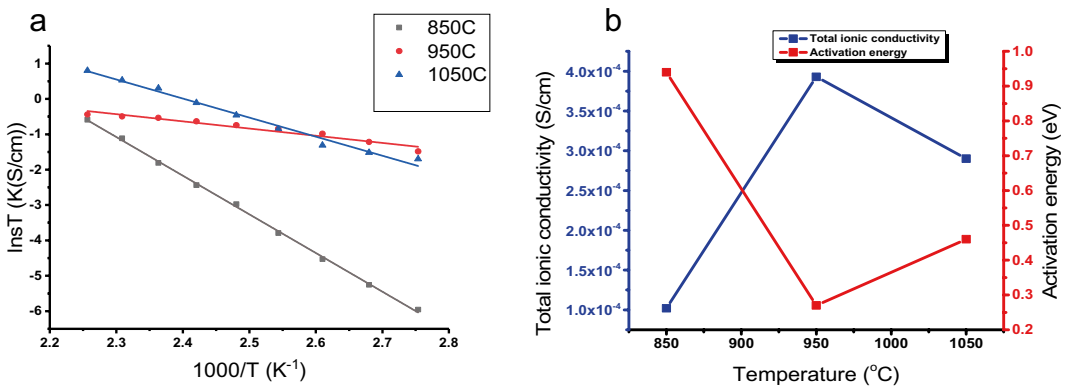

Figure 5. (**a**) Arhenius type plots of high temperature ionic conductivities for the determination of activation energies of the samples and (**b**) graph of total ionic conductivities and activation energy values as a function of sintering temperature.

Conclusion

In this work, SPS was successfully used for sintering and cubic phase stabilization, which was examined as a function of sintering temperature. Cubic LLZO phase was observed at temperatures as low as 850 °C, compared with higher temperature reported in the literature. The lattice parameters calculated from the Rietveld refinement analysis showed a decreasing trend as the sintering temperature increased. The SEM micrographs also show higher densification of particles with increased temperature, highlighting the increase in relative density from 94 to 99.9%. The ionic conductivity recorded in this work was 4.9×10^{-4} S/cm, which is among the highest values reported in the literature. Further optimization of the sintering parameters to reduce Li-deficit phases may enable higher conductivity values to be reached as well.

Acknowledgments

The authors would like to thank the Eskişehir Technical University Scientific Research Projects Unit for providing financial support through Grant No. 1802F030.

Data availability

Raw data were generated at Eskisehir Technical University Materials Science and Engineering laboratory. Derived data supporting the findings of this study are available from the corresponding author (Musah Abdulai) on request.

Declarations

Conflict of interest

The authors declare that the research was conducted in the absence of any commercial or financial relationships that could be interpreted as a potential conflict of interest.

REFERENCES

1. U.V. Alpen, A. Rabenau, G.H. Talat, Appl. Phys. Lett. **30**, 621–623 (1977)
2. A. Aatiq, M. Ménétrier, L. Croguennec, E. Suard, C. Delmas, J. Mater. Chem. **12**, 2971–2978 (2002)
3. F. Mizuno, A. Hayashi, K. Tadanaga, M. Tatsumisago, Solid State Ion. **177**, 2721–2725 (2006)
4. K. Takada, Acta Mater. **61**, 759–770 (2013). https://doi.org/10.1016/j.actamat.2012.10.034
5. Y. Wang, W.-H. Zhong, ChemElectroChem **2**, 22–36 (2015)
6. R. Murugan, S. Ramakumar, N. Janani, Electrochem. Commun. **13**, 1373–1375 (2011)
7. R. Murugan, V. Thangadurai, W. Weppner, Angew. Chem. Int. Ed. **46**, 7778–7781 (2007)
8. C. Bernuy-Lopez, W. Manalastas, J.M. LopezdelAmo, A. Aguadero, F. Aguesse, J.A. Kilner, Chem. Mater. **26**, 3610–3617 (2014)
9. D. Rettenwander, C.A. Geiger, M. Tribus, P. Tropper, G. Amthauer, Inorg. Chem. **53**, 6264–6269 (2014)
10. M. Huang, A. Dumon, C.-W. Nan, Electrochem. Commun. **21**, 62–64 (2012)
11. Q.-H.J. Ao Mei, Y.-H. Lina, C.-W. Nan, J. Alloys Compd. **486**, 871–875 (2009)
12. Y. Zhang, F. Chen, R. Tu, Q. Shen, X. Zhang, L. Zhang, Solid State Ion. **284**, 53–60 (2016)
13. J. Xue, K. Zhang, D. Chen, J. Zeng, B. Luo, Mater. Res. Express **70**, 25518 (2020)
14. M. Botros, 36–37 (2018)
15. M. Matsui, K. Takahashi, K. Sakamoto, A. Hirano, Y. Takeda, O. Yamamoto, N. Imanishi, Dalt. Trans. **43**, 1019–1024 (2014)
16. A. Castillo, T. Charpentier, O. Rapaud, N. Pradeilles, S. Yagoubi, Ceram. Int. **44**, 18844–18850 (2018)
17. L.C. Joong Sun Park, V. Zorb, A. Mehta, J. Cabana, G. Chen, M.M. Doeff, T. Richardson, J. Hoon Park, J.-W. Son, W.-Shick Hong, Thin Solid Film **572**, 55–60 (2015)
18. M.Y. Kotobuki, Binngong, L. Lu, H. Emil, M. Joanna, Funct. Mater. Lett. **9**, 359–365 (2016)
19. Z. Pan, W. La, Solid State Phenom. **281**, 767–773 (2018)
20. H. Buschmann, J. Dölle, S. Berendts, A. Kuhn, P. Bottke, M. Wilkening, P. Heitjans, A. Senyshyn, H. Ehrenberg, A. Lotnyk, V. Duppel, L. Kienle, J. Janek, Phys. Chem. Chem. Phys. **13**, 19378 (2011)
21. Y. Matsuda, K. Sakamoto, M. Matsui, O. Yamamoto, Y. Takeda, N. Imanishi, Solid State Ion. **277**, 23–29 (2015)